Predicting Supercell Motion Using a New Hodograph Technique

MATTHEW J. BUNKERS* AND BRIAN A. KLIMOWSKI

NOAA/NWS Weather Forecast Office, Rapid City, South Dakota

JON W. ZEITLER

NOAA/NWS Houston/Galveston Weather Forecast Office, Dickinson, Texas

RICHARD L. THOMPSON

NOAA/NWS Storm Prediction Center, Norman, Oklahoma

MORRIS L. WEISMAN

NCAR/Mesoscale and Microscale Meteorology Division, Boulder, Colorado

(Manuscript received 16 December 1998, in final form 13 September 1999)

ABSTRACT

A physically based, shear-relative, and Galilean invariant method for predicting supercell motion using a hodograph is presented. It is founded on numerous observational and modeling studies since the 1940s, which suggest a consistent pattern to supercell motion exists. Two components are assumed to be largely responsible for supercell motion: (i) advection of the storm by a representative mean wind, and (ii) propagation away from the mean wind either toward the right or toward the left of the *vertical wind shear*—due to internal supercell dynamics. Using 290 supercell hodographs, this new method is shown to be statistically superior to existing methods in predicting supercell motion for both right- and left-moving storms. Other external factors such as interaction with atmospheric boundaries and orography can have a pronounced effect on supercell motion, but these are difficult to quantify prior to storm development using only a hodograph.

1. Introduction

a. Background

Although supercells[1] have been given considerable attention since Browning (1964) first coined the term, arguably the least research effort has been directed toward predicting supercell motion. This is important since more than 90% of supercells are associated with some form of severe weather (i.e., tornadoes, flash flooding, hail $\geq$1.9 cm diameter, wind gusts $\geq$25 m s^{-1}, or wind damage) during their lifetime (e.g., Burgess and Lemon 1991). In addition, most strong or violent tornadoes are produced by supercells (e.g., Moller et al. 1994). Furthermore, knowledge of supercell motion has become increasingly important during the 1980s and 1990s as (i) both the research community and operational forecasters focused on storm-relative helicity (SRH) as a measure of supercell rotation and tornadic potential (Davies-Jones 1984; Davies-Jones et al. 1990; Davies and Johns 1993; Droegemeier et al. 1993; Johns et al. 1993), (ii) studies addressed storm-relative winds to discriminate between tornadic and nontornadic environments (Darkow and McCann 1977; Brooks et al. 1994a,b; Kerr and Darkow 1996; Stensrud et al. 1997; Thompson 1998), and (iii) anvil-level storm-relative flow has been used to broadly discriminate among low-precipitation (LP), classic (CL), and high-precipitation (HP) supercell environments (Rasmussen and Straka 1998)—which also has implications for tornado forecasting. These studies indicate that reliable prediction of supercell motion prior to storm development has the

[1] Supercells are defined similar to Moller et al. (1994)—convective storms with mesocyclones or mesoanticyclones. These storms are assumed to (i) have the absolute value of vertical vorticity be greater than or equal to 10^{-2} s^{-1}, (ii) persist at least on the order of tens of minutes, and (iii) be present through at least one-third of the convective storm's depth. Furthermore, right-moving supercells are defined as mesocyclones that move to the right of the vertical wind shear, and left-moving supercells are defined as mesoanticyclones that move to the left of the vertical wind shear.

Corresponding author address: Matthew J. Bunkers, NOAA/NWS Weather Forecast Office, 300 East Signal Drive, Rapid City, SD 57701-3800.
E-mail: Matthew.Bunkers@noaa.gov

potential to improve severe local storm warnings—implying the potential for saving lives and mitigating property loss. Thus, there is a need for a consistent and accurate method of predicting supercell motion.

b. Supercell motion and Galilean invariance

Theoretical and modeling studies have demonstrated that the internal processes that produce supercell motion within a horizontally homogeneous environment depend on the characteristics of the vertical wind shear, rather than just the characteristics of the wind (Rotunno and Klemp 1982, 1985; Weisman and Klemp 1982, 1984, 1986).[2] These processes are Galilean invariant, which is to say that the storm motion is the same, relative to the vertical wind shear, no matter where the vertical wind shear profile is positioned with respect to the origin of the hodograph. As an example, consider a moderate, unidirectionally sheared environment that leads to the development of symmetrically splitting supercells. Based on numerical modeling simulations, the internal dynamics promote storm propagation both to the right and to the left of the *vertical wind shear* for the cyclonic and anticyclonic storms, respectively. For a vertical wind shear profile in the upper-right quadrant of the hodograph (Fig. 1), this would generally lead to the cyclonic supercell moving slower and to the right of the mean wind and the anticyclonic supercell moving faster and to the left of the mean wind. Likewise, for the same vertical wind shear profile in the lower-right quadrant of the hodograph (Fig. 1), the cyclonic supercell would move faster and to the right of the mean wind while the anticyclonic member would move slower and to the left of the mean wind. Moreover, if the vertical wind shear profile were in the upper-left quadrant of the hodograph (Fig. 1), the cyclonic supercell would move to the left of the mean wind; however, this would still be to the right of the *vertical wind shear*. This Galilean invariance of the internal storm processes applies to curved wind shear profiles as well, with the caveat that cyclonic (anticyclonic) members of the split pair are favored for the clockwise-curved (counterclockwise curved) wind shear profiles, respectively.

The relative success of existing methods to predict supercell motion is due in some measure to the fact that, climatologically, vertical wind shear profiles in severe storm environments tend to reside predominantly within the upper-right quadrant of the hodograph. However, if the vertical wind shear profile is not as typical as this—

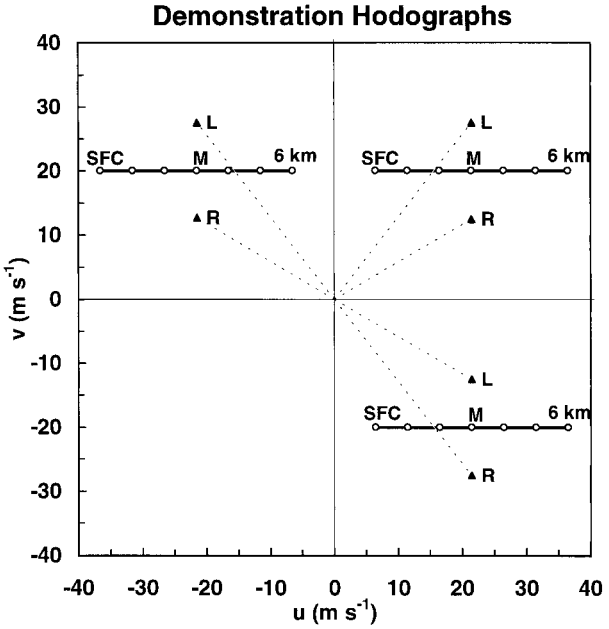

FIG. 1. Idealized 0–6-km hodographs (m s^{-1}) demonstrating the Galilean invariance relationship between supercell motion and the vertical wind shear for three unidirectional wind shear profiles. The cyclonic, right-moving (R) and anticyclonic, left-moving (L) supercell motions are noted for each of the three profiles with triangles; M denotes the 0–6-km mean wind. See section 1a for definition of supercells, and section 1b for discussion of Galilean invariance.

as often occurs in northwesterly flow situations or in tropical cyclone landfall scenarios (e.g., in the lower-right and upper-left quadrants of Fig. 1)—the storm motion algorithms that are not Galilean invariant will incorrectly represent the internal dynamical relationships described above and will, therefore, incorrectly forecast the supercell motion.

c. Existing methods for predicting supercell motion

Considerable research was conducted in the mid-1900s pertaining to thunderstorm motion (Byers 1942; Brooks 1946; Byers and Braham 1949; Newton and Katz 1958; Browning and Donaldson 1963; Browning 1964; Newton and Fankhauser 1964). It was generally observed that nonsevere thunderstorms moved with a representative mean wind, while stronger, larger, and longer-lived thunderstorms moved slower and to the right of the mean wind. In addition, some smaller and less frequently observed storms (yet still significant) were noted moving much faster and to the left of the mean wind (e.g., Achtemeier 1969). However, since knowledge of supercell dynamics was just emerging at that time, no consistently useful method to predict supercell motion was developed.

Various methods to predict supercell motion emerged during the 1970s. In a study of 159 tornado proximity soundings (not necessarily supercells), Maddox (1976, hereafter M76) estimated the storm motion at 75% of

[2] It is noted that mesoscale environments in and around supercells can be quite inhomogeneous. However, at present, numerical models cannot adequately represent horizontally inhomogeneous thunderstorm environments. Furthermore, the intent of this discussion is only to illustrate the importance of Galilean invariance with respect to supercell motion, which can be properly addressed given a horizontally homogeneous environment.

the mean wind speed and 30° to the right of the mean wind direction (hereafter denoted as 30R75). The mean wind was computed using the surface, and 850-, 700-, 500-, 300-, and 200-hPa winds. This 30R75 methodology was based on previous observations of severe storm deviant motion (Haglund 1969; Fankhauser 1971; Marwitz 1972a–c); however, no objective basis was presented for the choice of 30° or 75%. This method is relatively easy to compute, works well for typical North American supercell wind environments, and has been widely used as a basis for SRH calculations using both observational data and numerical model output. Unfortunately, this method is not Galilean invariant, and as such the prediction of supercell motion is not consistent for different vertical wind profiles with the same vertical wind shear. As a result, the 30R75 method produces less meaningful results as the vertical wind shear profile shifts toward the lower-left quadrant of the hodograph—typical of weaker wind environments. This is not physically consistent with observations or the model results discussed earlier.

Colquhoun (1980, hereafter C80) presented a method for estimating severe thunderstorm motion based on a balance of mass flux between the updraft and downdraft, with the following assumptions: (i) equal quantities of air are brought into the storm by the updraft and downdraft, and the upper limit of downdraft air is 450 hPa; (ii) maximum storm intensity is reached when it moves such that the rate of inflow of air to the updraft–downdraft system is maximized; and (iii) relative to the storm, the updraft approaches from the front and the downdraft from the back, or vice versa. Several iterations are required to compute storm motion, making it more computationally intensive than the other methods discussed herein. Most importantly, this method is not Galilean invariant. As an example, this method would predict exactly the same motion for an east–west (unidirectional) vertical wind shear profile with different displacements from the *x* axis (i.e., it predicts a right-moving supercell for $v > 0.0$ m s^{-1}, a left-moving supercell for $v < 0.0$ m s^{-1}, and no deviant motion for $v = 0.0$ m s^{-1}). The results presented in C80 indicate a 2.5 m s^{-1} mean absolute error (MAE; see Wilks 1995) in predicting the motion of 10 severe thunderstorms. Colquhoun and Shepherd (1989) applied this method when calculating thunderstorm motion in a study of an objective basis for forecasting tornado intensity.

Davies and Johns (1993, hereafter DJ93) modified M76's method for predicting supercell motion based on 31 central and eastern United States supercells comprising all seasons. Their motion is given by either (i) 30° to the right of the 0–6-km (all heights above ground level) mean wind direction at 75% of the mean wind speed if the mean wind speed is ≤15 m s^{-1} (30R75), otherwise (ii) 20° to the right of the 0–6-km mean wind direction at 85% of the mean wind speed (20R85). This method differs from M76 in stronger mean wind environments (i.e., >15 m s^{-1}) by reducing the deviation from the mean wind; it is also calculated over a shallower depth. DJ93 found that the motion of supercells varied widely with respect to the kinematic environment in which they formed, but decided that reasonably accurate forecasts of storm motion could be determined by using the above methodology. This method has since been used extensively to estimate supercell motion from both observed data and output from numerical weather prediction models. The DJ93 method has limitations similar to those of the M76 method.

Noting some deficiencies in the DJ93 method, Davies (1998, hereafter D98) expanded the DJ93 method for predicting supercell motion when the mean wind is relatively weak. In such cases, supercell motion has sometimes been observed to deviate by much greater than 30° to the right of the mean wind. D98's equation is calculated separately for three mean wind partitions: 0–10 m s^{-1}, 11–15 m s^{-1}, and >15 m s^{-1}. As with the M76 and DJ93 methods, the D98 method also is not Galilean invariant. This limitation is not as critical, however, as D98's results show improvement over application of a strict 30R75 estimate in weak mean wind environments. Most importantly, D98 highlighted the problem of computing storm-relative flow parameters using unrepresentative estimates of supercell motion.

Finally, Rasmussen and Blanchard (1998, hereafter RB98) presented a shear-relative method for predicting supercell motion; it is calculated as an 8.6 m s^{-1} deviation from the 0–0.5- to 4-km wind shear vector—orthogonal to the shear vector and starting at the point that is 60% of the magnitude of the shear. This was developed with 45 isolated supercell cases from the central and southern plains. Unlike the methods discussed above, this method is Galilean invariant, and most similar to the method proposed in the present paper. The supercells in RB98 were partitioned into LP, CL, and HP. The MAE was found to be within 4 m s^{-1} for LP and CL supercells. The HP supercells in the dataset deviated more strongly and in the direction of the low-level vertical wind shear (see also Rasmussen and Straka 1998).

d. Motivation for this research

The methods of predicting supercell motion discussed above, with the exception of RB98, generally work best for ''typical'' supercell environments when the vertical wind shear profile is primarily in the upper-right quadrant of the hodograph [e.g., Fig. 2a; also see Fig. 5 in Brown (1993)]. However, the non-Galilean invariant methods produce less desirable results for the ''atypical'' vertical wind shear profiles, which are shifted toward the lower-left quadrant of the hodograph, exhibit weak mean environmental winds, or have different orientations than what are more commonly observed (e.g., see Figs. 2b, 2c, and 2d, respectively). In addition to the weaknesses previously outlined, none of the above methods account for left-moving supercells (e.g., Fig.

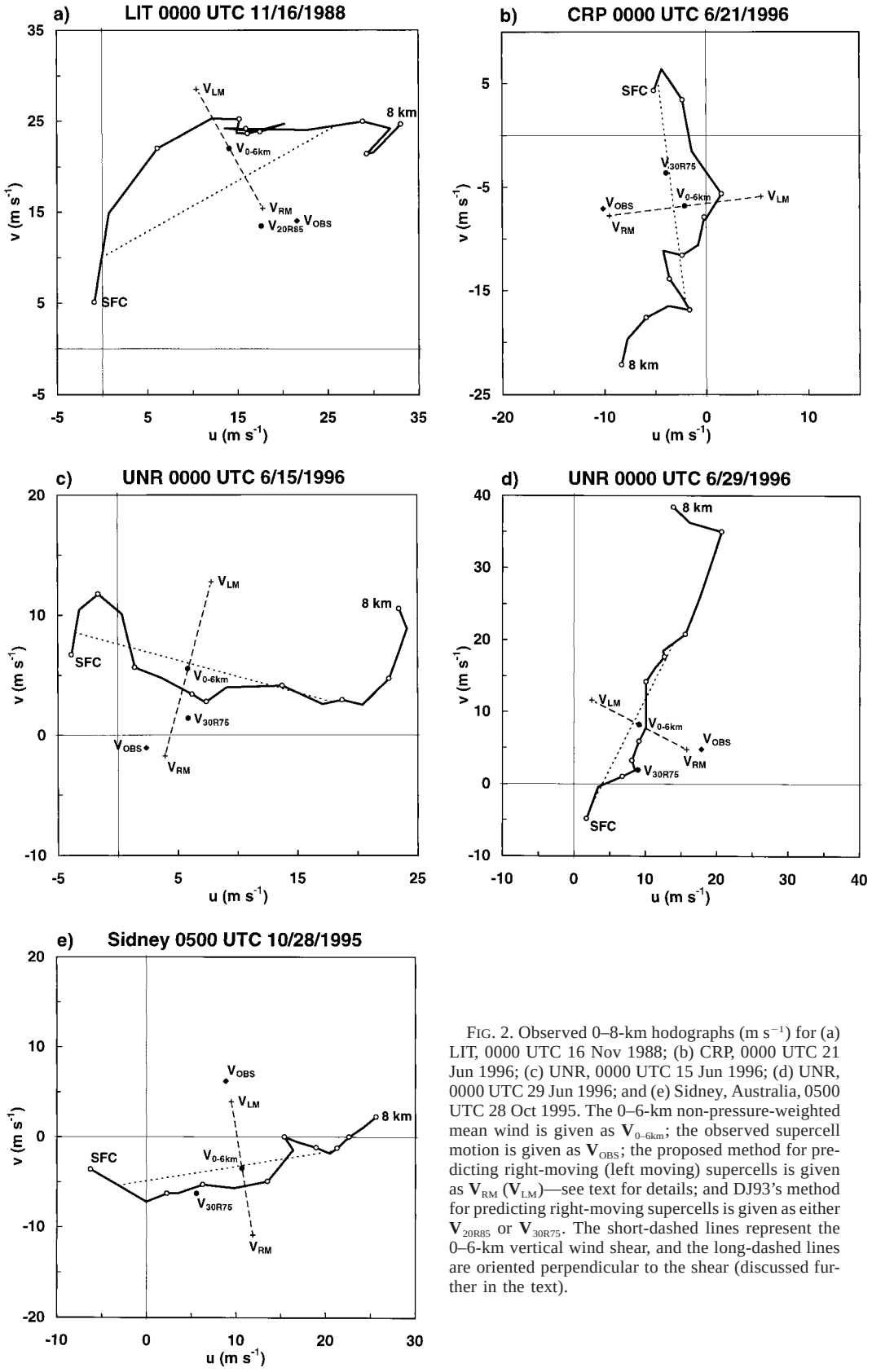

FIG. 2. Observed 0–8-km hodographs (m s^{-1}) for (a) LIT, 0000 UTC 16 Nov 1988; (b) CRP, 0000 UTC 21 Jun 1996; (c) UNR, 0000 UTC 15 Jun 1996; (d) UNR, 0000 UTC 29 Jun 1996; and (e) Sidney, Australia, 0500 UTC 28 Oct 1995. The 0–6-km non-pressure-weighted mean wind is given as $\mathbf{V}_{0\text{–}6\text{km}}$; the observed supercell motion is given as $\mathbf{V}_{\text{OBS}}$; the proposed method for predicting right-moving (left moving) supercells is given as $\mathbf{V}_{\text{RM}}$ ($\mathbf{V}_{\text{LM}}$)—see text for details; and DJ93's method for predicting right-moving supercells is given as either $\mathbf{V}_{20\text{R}85}$ or $\mathbf{V}_{30\text{R}75}$. The short-dashed lines represent the 0–6-km vertical wind shear, and the long-dashed lines are oriented perpendicular to the shear (discussed further in the text).

2e); however, it should be noted that these studies did not focus on left-moving supercells since almost all tornadoes are produced by right-moving supercells. Moreover, the method of C80 does predict left-moving supercells for certain atypical vertical wind shear profiles, such as described earlier, but it does not account for the simultaneous occurrence of both right- and left-moving supercells; the method of RB98 could easily be extended to account for left-moving supercells. Although left-moving supercells are less frequent than right-moving supercells in the United States, they are sometimes favored in other parts of the world [e.g., Australia—Dickins (1994)]. Therefore, a Galilean invariant method for simultaneously predicting both right- and left-moving supercells is desired.

The literature suggests that one should be able to develop a more physically based method to predict supercell motion. Weisman and Klemp (1986) identified two main factors that determine supercell motion:

- advection of the storm by the mean wind, and
- motion resulting from interaction of a convective updraft with the vertically sheared environment (see Rotunno and Klemp 1982, 1985; Klemp 1987).

Modeling studies of supercells under various vertical wind shear and buoyancy profiles support this premise (Klemp and Wilhelmson 1978; Weisman and Klemp 1984, 1986; Rotunno and Klemp 1982, 1985; Droegemeier et al. 1993), as do various observational studies of supercell hodographs (Newton and Fankhauser 1964; Chisholm and Renick 1972; Marwitz 1972a–c; Darkow and McCann 1977; Fankhauser and Mohr 1977; Bluestein and Parks 1983; Bluestein and Jain 1985; Brown 1993). In these examples, mean supercell motion was generally 4 to 12 m s^{-1} to the right (or left) of the mean wind along a line roughly perpendicular to the vertical wind shear. This deviant motion is largely due to favorable dynamic vertical pressure gradient forcing produced on the storm flanks as a result of updraft rotation—which arises from tilting of horizontal vorticity into the updraft. Weisman (UCAR 1996) presented a new method to estimate supercell motion based on these observations, whereby movement was estimated as 3 to 8 m s^{-1} away from the 0–6-km pressure-weighted mean wind, and perpendicular to the 0–6-km vertical wind shear vector.

Due to the various shortcomings of some of the existing methodologies for predicting supercell motion, Bunkers et al. (1998) expanded upon Weisman's (UCAR 1996) method to predict supercell motion using hodograph data for 125 right-moving supercells; what follows is an extension of that work. Hereafter this method is referred to as the internal dynamics (ID) method since it is physically based on the internal dynamics of the supercell (as opposed to external dynamics). The ID method is also shear relative and Galilean invariant; however, it should be noted that it is still an empirical method based on a dataset of supercells. In light of the above discussion, the objectives of this study are (i) to test the ID method in predicting both right- and left-moving supercell motion using a large set of observed cases, (ii) to compare the ID method to some existing methods for predicting supercell motion, and (iii) to make recommendations on ways to estimate supercell motion.

2. Data and methodology

a. Supercell data

1) DATA DEVELOPMENT

Supercell hodographs and motions were gathered from a wide variety of sources. The primary data source consisted of 138 right-moving supercell occurrences and motions from Thompson (1998) spanning 1995 to 1996—nearly all from the central and eastern United States. Second, 33 right-moving supercell hodographs and motions were obtained from Brown (1993). An additional 31 right-moving supercell occurrences and motions were obtained from DJ93. A review of the meteorological literature generated 39 right-moving and 23 left-moving supercell occurrences and motions from 1962 to 1998 (see Tables A1 and A2 in the appendix). Finally, 57 right-moving and 7 left-moving supercell occurrences and motions were obtained—mostly across the northern Great Plains—from 1995 to 1999 using the Weather Surveillance Radar-1988 Doppler (WSR-88D) archived data.

Since the supercells from Thompson (1998) fell within ± 3 h of sounding release time, no attempt was made to modify individual soundings. The spatial criteria used in deriving a representative hodograph for supercells in Thompson (1998) were as follows: (i) the unmodified sounding in the low-level inflow region of the supercell was used in calculating supercell motion estimates; (ii) if the inflow sounding was missing or unrepresentative (i.e., contaminated by convection or dryline passage), the next closest sounding was interrogated and possibly used; and (iii) if the supercell was equidistant from sounding locations, the u and v components of the corresponding wind profiles were averaged to produce a composite hodograph.

The hodographs provided by Brown (1993) were used without modification. Similarly, the DJ93 soundings were not modified; however, if more than one sounding was listed for a particular case, the u and v components of the corresponding wind profiles were averaged to produce a composite hodograph. Soundings from the review of meteorological literature were not modified, and were chosen based on a temporal constraint of ± 3 h from sounding release time. The soundings and storm motions for the supercells obtained from the WSR-88D archived data were also calculated similar to Thompson (1998). In addition, Wind Profiler Demonstration Network (WPDN) vertical wind profile data, WSR-88D vertical wind profile data, and surface wind data were used

to develop or modify hodographs for 10 of the supercell cases.

All necessary sounding data were retrieved either from the National Climatic Data Center Radiosonde Data of North America 1946–1995 CD-ROM or from the online archive provided by the Forecast Systems Laboratory for post-1995 data (http://raob.fsl.noaa.gov). There were several cases in which soundings were missing or nonrepresentative, resulting in a smaller number of digitized hodographs than supercell occurrences. The complete dataset consists of 290 supercell hodographs at 500-m intervals from the surface to 8 km, along with the supercell motion; 260 hodographs are for right-moving supercells, 30 are for left-moving supercells.

Since the cases used in the present study span a variety of sources, several different methods have been used to calculate observed supercell motion. This introduced potential error into the combined dataset. However, most supercell motions were calculated (i) by tracking the centroid of the supercell, (ii) during the most intense phase of the supercell (or when it was tornadic), (iii) for a period on the order of an hour, and (iv) when the supercell was separated from other storms by several tens of kilometers. The size of the dataset and isolation of most of the supercells indicate that comparison of the various methods used to predict supercell motion outlined above (section 1c) should not suffer from the use of more than one method to calculate observed supercell motion. Moreover, the errors in the observed storm motion should be random—not systematic.

Another potential data concern arose because the spatial criteria for developing hodographs in this study were not as strict as in previous studies (e.g., Darkow 1969). Again, this should not be problematic because (i) the goal of this procedure was to obtain a representative background vertical wind shear profile of the supercell environment and not a tornado/supercell proximity sounding, (ii) a relative comparison of the supercell motion algorithms was being made with the same dataset, and (iii) nearly all of the soundings used were in the inflow region to the supercell. Furthermore, Weisman et al. (1998) showed that significant modifications to a storm's local environment can extend out as far as 30 km, suggesting near-storm environments may not be the best choice for a representative sounding. For a more thorough discussion on the methods, difficulties, and caveats of choosing representative soundings, see Brooks et al. (1994a).

2) DATA PARTITIONING

The dataset of 260 right-moving supercells was subdivided into a development dataset and a verification dataset; each consisted of 130 cases. This was accomplished with a random number generator. The development dataset was used to set the values of the parameters (discussed in section 2b below) for the ID method, and the verification dataset was used for comparison of the various methods used to predict supercell motion.

Additionally, in light of the perceived inadequacies of the methods that are not Galilean invariant, the verification dataset was partitioned to differentiate between cases when the methods based on the mean wind resulted in the smallest forecast errors (i.e., vertical wind shear profiles in the upper-right quadrant of the hodograph), and cases when these methods were not as effective (i.e., vertical wind shear profiles that were shifted toward the lower/left quadrants of the hodograph). After examining the many supercell hodographs available for this study, atypical hodographs were arbitrarily defined as either (i) those with a 0–6-km mean wind <10.0 m s^{-1}, or (ii) those with both a northerly surface wind and an absolute value of the magnitude of the surface wind >5 m s^{-1}. If neither criteria i nor ii were satisfied, the hodograph was classified as typical.

These criteria were intended to highlight environments when either the mean wind was relatively weak (e.g., Fig. 2c) or when the flow pattern represented a nontypical synoptic situation such as northwest flow (e.g., Fig. 2b; Johns 1984) or postfrontal supercells (e.g., Fig. 2d). It is also important to note the classifications were not based on the shape of the vertical wind shear profile; rather, they were based on the orientation of the vertical wind shear profile relative to the origin of the hodograph. This was supported by numerous observations of supercell hodographs (e.g., Chisholm and Renick 1972; Brown 1993). The methods used to forecast supercell motion were critiqued for the verification dataset, and also for the verification dataset partitioned into typical and atypical cases.

3) SOME OBSERVATIONS OF THE ENTIRE RIGHT-MOVING SUPERCELL DATASET

There was a wide range of deviations of the observed supercell motion from the 0–6-km mean wind, varying from 3.0 to 18.5 m s^{-1} (Fig. 3); the interquartile range was 6.6 to 10.3 m s^{-1}. There was only a very slight tendency for the supercell motion to deviate more strongly from the 0–6-km mean wind as the 0–6-km shear magnitude increased (Fig. 3a; r = correlation coefficient = 0.16). The results for the 0–3-km shear magnitude were similar to those for the 0–6-km shear magnitude (not shown). There was, however, a greater tendency for the supercell motion to deviate more strongly from the 0–6-km mean wind as the 0–3-km SRH increased (Fig. 3b; $r = 0.48$). [The 0–6-km shear magnitude was calculated as the length of the vertical wind shear profile, and the 0–3-km SRH was calculated as in Davies-Jones et al. (1990).] Finally, there was also very little correlation between the strength of the 0–6-km mean wind and the deviation of the supercell motion from the mean wind (Fig. 3c; $r = 0.16$).

Figure 3 illustrates the difficulty inherent in predicting supercell motion. For example, similar deviations from

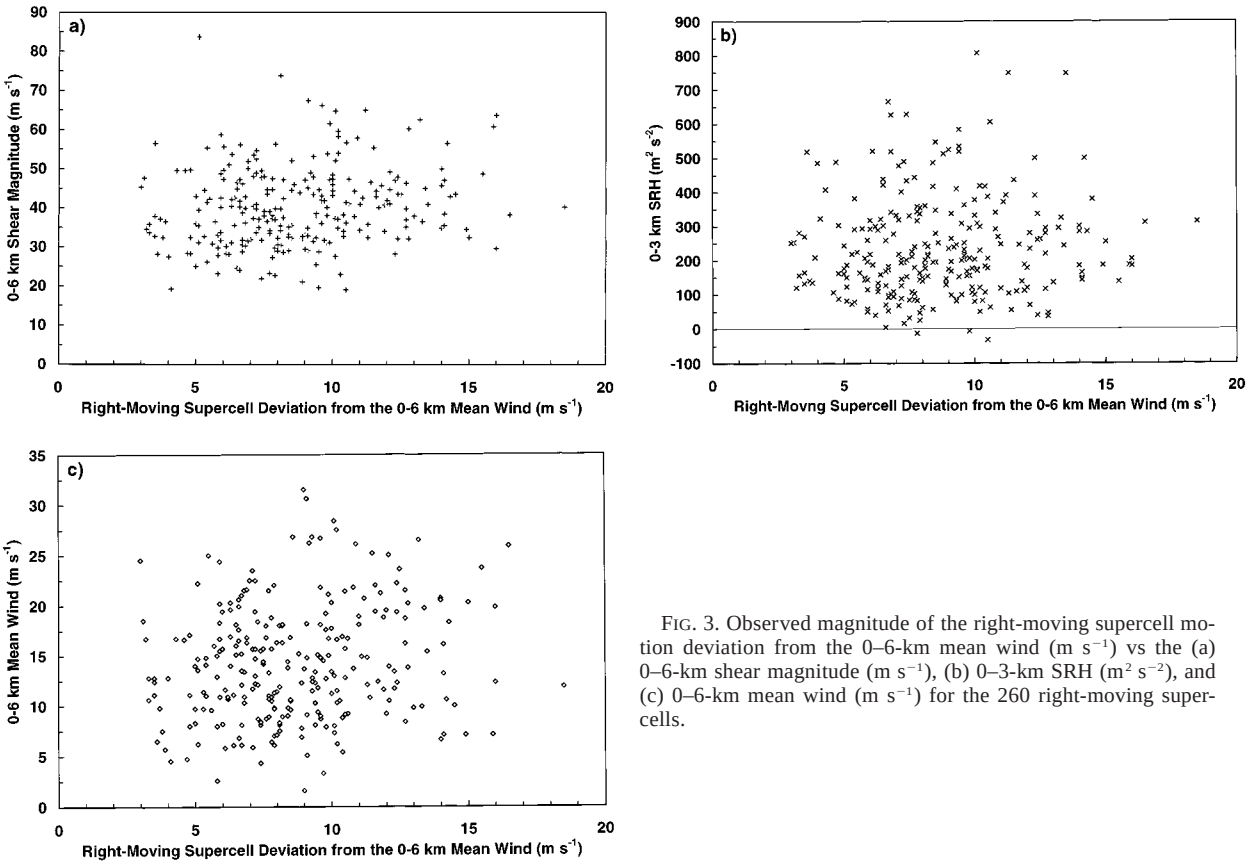

FIG. 3. Observed magnitude of the right-moving supercell motion deviation from the 0–6-km mean wind (m s^{-1}) vs the (a) 0–6-km shear magnitude (m s^{-1}), (b) 0–3-km SRH (m^2 s^{-2}), and (c) 0–6-km mean wind (m s^{-1}) for the 260 right-moving supercells.

the mean wind occurred for both moderate and strong wind shear cases, and there was no predictive capability in determining this deviation based solely on the 0–6-km shear magnitude (Fig. 3a). Although there was an association between larger 0–3-km SRH values and greater deviations from the 0–6-km mean wind (Fig. 3b), SRH is dependent on storm motion and as such this result is likely a consequence of a storm motion being highly deviant—again providing little predictive capability. Other studies have suggested that supercell motion deviates more strongly from the mean wind for weak mean wind environments (e.g., DJ93, D98); however, very little evidence for this exists here (Fig. 3c). In fact, the data show a tendency for the larger deviations from the mean wind as the mean wind speed increased. This does not address the directional deviation, which in fact does turn out to be greatest in weak mean wind environments. It is difficult to determine what specifically caused this wide range of deviations from the mean wind, but there likely were a combination of factors—both internal and external to the storm—that were influencing the supercell motion.

Although Fig. 3 offers very little predictive capability in determining the deviation of the supercell motion from the mean wind, it does offer some insight into supercell environments. First, the 0–6-km shear magnitude was greater than 19.0 m s^{-1} for all supercell cases, and was greater than 20 (26) m s^{-1} for 99% (95%) of the supercell cases (Fig. 3a). The 0–3-km SRH was negative for only three of the right-moving supercell cases, but did fall between 0 and 100 m^2 s^{-2} for 38 (15%) of the supercell events, and was greater than 150 m^2 s^{-2} for 175 (67%) of the events (Fig. 3b). Although Fig. 3b cannot be directly compared to the results of Davies-Jones et al. (1990) because of differences in the datasets involved (i.e., not all cases are tornadic in the current study), it appears that right-moving supercells can occur when the observed SRH falls well below their rough suggested guideline of 150 m^2 s^{-2}. On the other hand, forecasters should strongly consider the 0–6-km shear magnitude when determining the potential for supercells, with values $\geq$20 m s^{-1} being favorable for development. It is important to note that the values of SRH and, to a lesser extent, shear magnitude, are dependent upon the resolution of the dataset used (Markowski et al. 1998b). See RB98 for a more detailed discussion on supercell environments.

b. The internal dynamics method for predicting supercell motion

Under the assumption that supercell motion can be described by the sum of both an advective component

and a propagation component—owing to internal supercell dynamics, in the absence of other external factors—the equation for the motion of a right-moving supercell ($\mathbf{V}_{RM}$) can be expressed in vector form as

$$\mathbf{V}_{RM} = \mathbf{V}_{mean} + D\left[\frac{\mathbf{V}_{shear} \times \hat{\mathbf{k}}}{|\mathbf{V}_{shear}|}\right]. \quad (1)$$

The mean wind vector (or advective component) is given by $\mathbf{V}_{mean}$, the vertical wind shear vector is given by $\mathbf{V}_{shear}$, and D represents the magnitude of the deviation of the supercell motion from the mean wind, constrained to be along a line orthogonal to the vertical wind shear vector. Values for these three parameters ($\mathbf{V}_{mean}$, $\mathbf{V}_{shear}$, and D) are defined in section 3a based on the present development dataset. By reversing the cross product in Eq. (1), the equation for the motion of a left-moving supercell ($\mathbf{V}_{LM}$) can similarly be expressed in vector form as

$$\mathbf{V}_{LM} = \mathbf{V}_{mean} - D\left[\frac{\hat{\mathbf{k}} \times \mathbf{V}_{shear}}{|\mathbf{V}_{shear}|}\right]. \quad (2)$$

The bracketed terms in Eqs. (1) and (2) are unit vectors orthogonal to $\mathbf{V}_{shear}$, either to the right ($\mathbf{V}_{RM}$) or to the left ($\mathbf{V}_{LM}$) of the vector. Multiplying the bracketed terms by D results in the propagation components.

Referring back to the hodographs in Fig. 2, the short-dashed lines represent the vertical wind shear (as defined in section 3a below); the long-dashed lines are orthogonal to the shear and pass through the mean wind. The first components of Eqs. (1) and (2) are expressed by the 0–6-km non-pressure-weighted mean wind (for reasons discussed in section 3a); the second components of Eqs. (1) and (2) are expressed as an offset from the mean wind in a direction along the long-dashed line—to the right (*relative to the vertical wind shear*) for a cyclonic supercell and to the left for an anticyclonic supercell. This is defined as the ID method.

The parameters ($\mathbf{V}_{mean}$, $\mathbf{V}_{shear}$, and D) for the ID method described above must be specified (e.g., empirically derived) in order to calculate supercell motion. In order to specify these parameters, a brute force approach was taken by calculating the MAEs between the observed and predicted supercell motion by varying the methods used to compute the mean wind and vertical wind shear, and by varying the magnitude of the deviation, D, from the mean wind. This resulted in several iterations of Eq. (1) being performed on the 130 right-moving supercell development dataset. First, the layer used to calculate the mean wind was varied from 0–4 to 0–8 km at 1-km increments; both pressure weighting and non–pressure weighting were employed. For each mean wind layer used, the deviation, D, was varied from 4 to 12 m s^{-1} at 0.5 m s^{-1} increments. Finally, the head (tail) of the vertical wind shear vector was varied from one data level—starting at the top (bottom) of the mean wind layer—to one-half the depth of the mean wind layer, while keeping the tail (head) of the vertical wind shear vector held fixed. For example, using the 0–6-km layer, the head of the vertical wind shear vector was varied from 6 km, 5.5–6 km, 5–6 km, . . . , 3–6 km. For the 0–4-km mean wind layer, these iterations resulted in 850 total computations to find the minimum MAE (425 each for the pressure-weighted and non-pressure-weighted mean wind), and for the 0–8-km mean wind layer, this resulted in 2754 total computations.

After the ID method was empirically tuned with the 130 right-moving supercell *development* dataset, forecast movements for the ID method were compared with those of M76, C80, DJ93, D98, and RB98 using the 130 right-moving supercell *verification* dataset. Afterward, the results for the right-moving supercells were extended to the 30 hodographs for left-moving supercells. The Student's *t*-test was used to assess significance by evaluating the mean of the differences of absolute errors for the varying methods used to predict supercell motion (Milton and Arnold 1990; Wilks 1995). The appropriate test statistic is given as

$$T = \frac{\overline{d} - 0}{S_d/\sqrt{n}}. \quad (3)$$

The random variable, d, is defined as the difference of absolute errors for the paired observations ($X_i - Y_i$; $i = 1, \ldots, n$); $\overline{d}$ is the mean of these differences; and S_d is the standard deviation of these differences. For the purposes of this study, X_i is defined as the set of absolute errors for the ID method ($n = 130$), and Y_i as the set of absolute errors for each of the other methods. The null hypothesis (H_0: $\mu_d = 0$) was rejected in favor of the alternative hypothesis (H_A: $\mu_d < 0$) if the test statistic fell in the lowest 1% ($\alpha = 0.01$) of the t distribution (i.e., this is a left-tailed test). Here, μ_d represents the theoretical mean value for d over the entire population, and α represents the probability of falsely rejecting the null hypothesis, given that it is true. This test requires the differences, d, both to follow a Gaussian distribution and to be independent. These are reasonable assumptions for this study since the central limit theorem is applicable and the supercells occurred over a broad temporal and spatial scale, with lag-1 autocorrelations <0.10.

3. Results and discussion

a. Optimizing the ID method for right-moving supercells

Using the ID method, the minimum MAE in predicting supercell motion for the 130 right-moving supercell development dataset was 4.1 m s^{-1} for both the pressure-weighted and non-pressure-weighted mean wind. This minimum occurred for the 0–6-km non-pressure-weighted mean wind layer (Table 1), and also for the 0–7- and 0–8-km pressure-weighted mean wind

TABLE 1. Minimum mean absolute errors (MMAE) in predicting supercell motion with the ID method for the 130 right-moving supercell development dataset using the non-pressure-weighted mean wind (MW) for the 0–4- to 0–8-km layers at 1-km increments under varying deviations (D) from the mean wind. ''Head'' (''tail'') represents the level/layer used in calculating the head (tail) of the vertical wind shear vector. The highlighted values are those chosen for optimizing the ID method, discussed further in the text.

MMAE (m s^{-1})	MW (km AGL)	D (m s^{-1})	Head (km AGL)	Tail (km AGL)
5.1	0–4	8.5	2.0–4.0	0.0
4.4	0–5	7.5	5.0	0.0
4.1	***0–6***	***7.5***	***5.5–6.0***	***0.0–0.5***
4.3	0–7	7.0	3.5–7.0	0.0–1.0
4.9	0–8	7.5	4.0–8.0	0.0–1.5

layers (not shown). The deviation, *D*, which minimized the MAE, ranged from 7.0 to 8.5 m s^{-1}. This is consistent with the clustering of supercell motion deviation from the 0–6-km mean wind around 8.5 m s^{-1} in Fig. 3. Based on these results, the following parameters were used in Eq. (1) to predict supercell motion via the ID method:

- a 0–6-km non-pressure-weighted mean wind,
- a deviation from the 0–6-km mean wind of 7.5 m s^{-1},
- a 5.5–6-km mean wind for the head of the vertical wind shear vector, and
- a 0–0.5-km mean wind for the tail of the vertical wind shear vector.

The 0–7- and 0–8-km pressure-weighted mean wind layers were rejected because they required more information (pressure and additional wind data) and calculations with no apparent reduction in the minimum MAE.

Choosing just one set of these parameters is, admittedly, a simplistic approach to predicting supercell motion. First, 0–6 km is not always going to be the most representative layer for computing the mean wind or vertical wind shear. There are situations when a shallower layer may be more appropriate, such as with mini-supercells (Davies 1993), supercells over mountainous terrain (Keighton and Passetti 1998), or supercells in landfalling tropical cyclones (McCaul 1991; McCaul and Weisman 1996). There are also some cases in which a deeper layer may be more appropriate, such as environments with *extreme* buoyancy and a deep troposphere (Korotky et al. 1993), or *elevated* supercells on the cold side of a boundary. A representative mean wind depth in a given situation might be determined by noting the height of the equilibrium level, the depth of the buoyant energy on a sounding, or the height of maximum buoyancy on a sounding—as suggested by D98. Making the depth of the mean wind a function of one of these parameters has the potential to reduce the MAE in predicting supercell motion. Whether or not this additional information would be worth the extra calculations involved remains to be seen; this is a subject of future research.

Second, although the deviation (*D*) could be altered for different environments, the results above suggest this might not be desirable. It is not clear why some supercells deviate significantly from the mean wind, while others do so to a much lesser degree. Reasons for the deviations from the mean wind by greater than 10 m s^{-1} might be related to both the effects of the storm outflow and interactions with preexisting atmospheric boundaries. Rasmussen and Straka (1998) provided evidence that HP supercells are more likely to deviate strongly from the mean wind than other types of supercells. On the other end of the spectrum, there is only limited evidence to suggest that deviations are smaller in low shear and low SRH environments (recall Figs. 3a,b). The weaker shear and SRH may result in weaker mesocyclones, which, in turn, are associated with weaker dynamically induced updrafts (i.e., a smaller propagation component).

b. Comparison of the ID method with other methods

Based on the verification dataset of 130 right-moving supercells, the ID method was statistically superior to the other identified methods in terms of having the smallest MAE between the observed and predicted supercell motion (Table 2a). The MAE was about 1 m s^{-1} less for the ID method relative to the other methods, except for C80, in which the ID method resulted in a 2.2 m s^{-1} improvement. These results were statistically significantly at $\alpha = 0.01$ (also at $\alpha = 0.0005$) based on the Student's *t*-test for comparing paired data. Moreover, the ID method provided the best forecast (i.e., smallest MAE) of supercell motion 63% to 75% of the time when compared head to head to the other methods—26% when all other methods were considered collectively. The ID method was generally superior in minimizing the error and bias in both the direction of supercell motion and the 0–3-km SRH. The interquartile range of the absolute errors was also the smallest for the ID method (i.e., smallest box in Fig. 4a). Finally, the results using the root-mean-square error (rmse) were similar to the MAE (not shown).

The effectiveness of the methods of RB98, D98, DJ93, and M76 appeared quite similar in terms of both the MAE and the distribution of the absolute errors (Table 2a, Fig. 4a). This was not surprising for DJ93 and M76, but it was somewhat surprising for RB98 and D98; the RB98 method is Galilean invariant and was expected to perform better than the methods that are not Galilean invariant; the D98 method is a modification of DJ93 and as such it would be expected to provide an improvement over DJ93. Also note the MAE for RB98's method was greater for this dataset than what they reported for their dataset; this occurred because the present study included all types of supercells (i.e., CL, HP,

TABLE 2a. Comparison statistics between the ID method and the other methods discussed in the text for the 130 right-moving supercell verification dataset. The ''best predicted'' row indicates the percentage of the time when the individual algorithms were superior to the ID method. Various reference p values for the Student's *t*-test are $\alpha_{0.05} = -1.645$, $\alpha_{0.01} = -2.326$, and $\alpha_{0.0005} = -3.291$.

	ID	RB98	D98	DJ93	M76	C80
MAE (m s^{-1})	**4.1**	5.1	5.5	4.9	5.1	6.3
Student's *t*-test	—	−5.81	−5.19	−4.40	−4.68	−8.37
Best predicted (%)	—	32	29	37	36	25
Theta error (°)	11	17	15	14	14	23
Theta bias (°)	−2	9	−6	−9	−5	−6
SRH error (m^2 s^{-2})	39	48	53	52	52	67
SRH bias (m^2 s^{-2})	−12	13	−30	−36	−18	−27

and LP), while they omitted HP supercells from their calculations.

Upon partitioning the 130 right-moving supercell verification dataset, 95 (73%) typical and 35 (27%) atypical hodographs were classified; see definition in section 2a. For the typical hodographs, the ID method exhibited only a 0.4–0.6 m s^{-1} improvement over the DJ93 and M76 methods, with a 1–2 m s^{-1} improvement over the others (Table 2b). The superiority of the ID method was statistically significant at the $\alpha = 0.01$ level compared with all other methods except DJ93. Furthermore, the ID method was superior in predicting supercell motion for the typical hodographs 56% to 72% of the time when compared head to head to the other methods (24% when all other methods were considered collectively), with the least improvement when compared to the methods of DJ93 and M76. The distribution of absolute errors was quite similar for the ID, DJ93, and M76 methods, although the ID method still possessed the smallest interquartile range (Fig. 4b).

The above results were expected since the methods of DJ93 and M76 were based largely on upper-right quadrant hodographs, and that is what the hodographs in the typical partition mostly represent. The fact that the ID method was comparable to and/or produced slightly improved results over the methods based on the mean wind for this subset was encouraging. The MAEs for the other methods (RB98, D98, and C80) remained relatively unchanged for this partitioning (cf. Tables 2a and 2b).

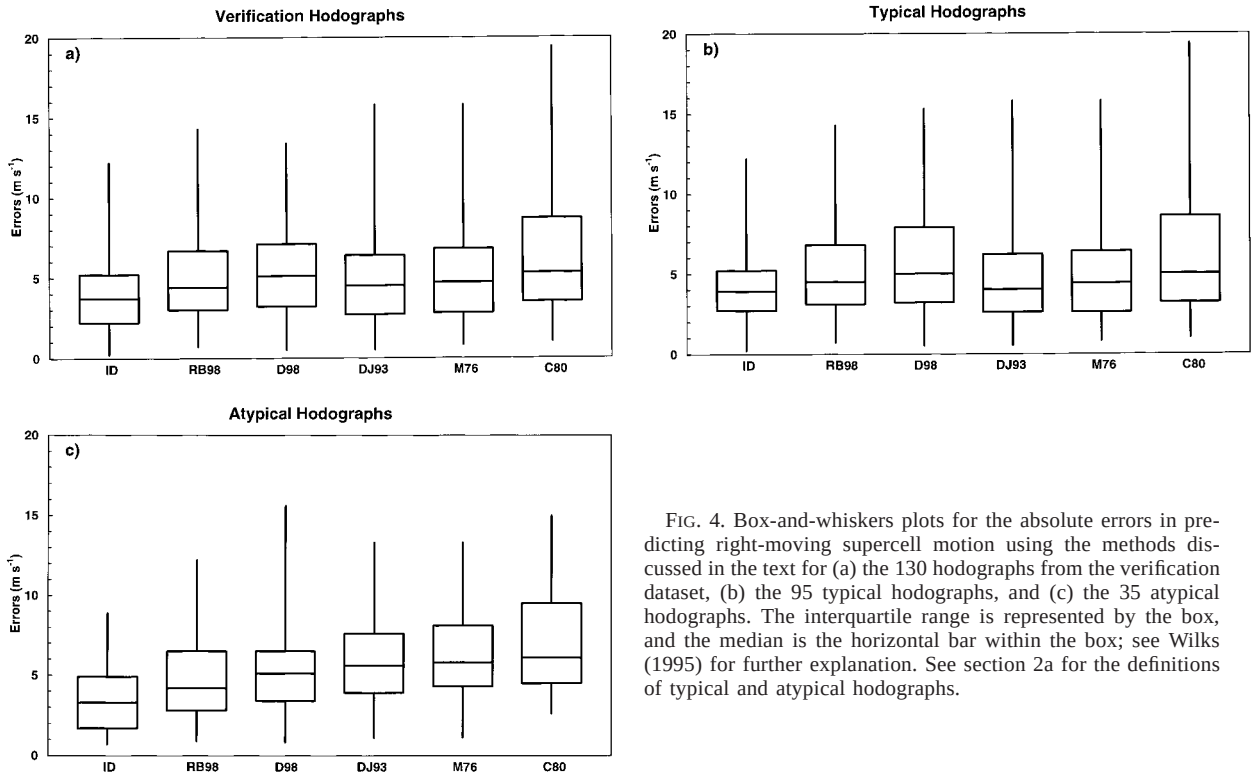

FIG. 4. Box-and-whiskers plots for the absolute errors in predicting right-moving supercell motion using the methods discussed in the text for (a) the 130 hodographs from the verification dataset, (b) the 95 typical hodographs, and (c) the 35 atypical hodographs. The interquartile range is represented by the box, and the median is the horizontal bar within the box; see Wilks (1995) for further explanation. See section 2a for the definitions of typical and atypical hodographs.

TABLE 2b. Same as Table 2a but for the 95 typical supercell hodographs; see section 2a for definition of a typical hodograph.

	ID	RB98	D98	DJ93	M76	C80
MAE (m s^{-1})	**4.2**	5.2	5.5	4.6	4.8	6.1
Student's t-test	—	−4.40	−4.07	−1.86	−2.35	−5.97
Best predicted (%)	—	32	28	44	43	29
Theta error (°)	10	14	13	11	12	21
Theta bias (°)	−3	6	−9	−6	−1	1
SRH error (m^2 s^{-2})	41	49	56	47	48	59
SRH bias (m^2 s^{-2})	−13	13	−37	−26	−2	−6

The most statistically significant improvements occurred for the atypical hodograph partitioning. The MAE was 3.6 m s^{-1} for the ID method, which ranged from 1.2 to 3.4 m s^{-1} lower than for the other methods (Table 2c). The largest improvement using the ID method and the atypical hodograph partitioning occurred with respect to the methods based on the mean wind (and also C80), and the smallest improvement was noted with respect to the RB98 method. The DJ93 and M76 methods produced much greater MAEs with the atypical hodographs than was the case with the typical partitioning (cf. Tables 2b and 2c). The ID method most accurately predicted the supercell motion 69% to 89% of the time when compared head to head to the other methods (31% when all other methods were considered collectively). Also apparent from these results was how the methods of DJ93, M76, and C80 exhibited a substantial negative bias for both the direction of storm motion and 0–3-km SRH. The atypical partitioning produced smaller MAEs with the methods of RB98 and D98 when compared to the methods of DJ93 and M76. Finally, the distribution of absolute errors for the ID method was clearly different from the other methods, with the 50th (75th) percentile for the ID method below the 25th (50th) percentile for all other methods except RB98 (Fig. 4c).

These results can be explained by understanding the nature of the various methods used to predict supercell motion. First, the RB98 method is both shear relative and Galilean invariant, similar to the ID method. Even though it does not utilize the same two components as does the ID method, it is inherently similar. Therefore, it is expected to perform better than the methods based on the mean wind in atypical hodograph environments. Second, the D98 method—although still based on the mean wind—was developed using hodographs from weak mean wind environments in an attempt to account for large angular deviations from the mean wind, hence the modest improvement. The greatest weakness of both the DJ93 and M76 methods is their lack of Galilean invariance; thus, they performed most poorly for the atypical hodograph partitioning when compared to the other partitions. The larger errors produced by the C80 method may be explained by its dependency on hodograph orientation in determining whether a right- or left-moving supercell is predicted.

Composite hodographs for both the typical and atypical supercell datasets did not reveal any significant differences in vertical wind shear between the two environments (Fig. 5). These hodographs were developed by (i) translating the origin of the hodograph to the point defined by the 0–0.5-km mean wind, and (ii) rotating the hodograph such that the vertical wind shear (as defined above for the ID method) was positive and along the abscissa. This simpler compositing procedure was selected in favor over that of Brown (1993) due to the size of the dataset. This was not expected to compromise the results since the comparison was relative and not absolute. For the typical (atypical) composite hodograph the 0–6-km shear magnitude was 28.2 (26.5) m s^{-1} and the 0–3-km SRH was 222 (176) m^2 s^{-2}. The difference between the composite storm motions for these two datasets was only 0.4 m s^{-1}. There does not appear to be any fundamental reason why supercell motion would be different, with respect to the shear profile, for the atypical hodograph environments as opposed to the typical hodograph environments. This underscores the importance of Galilean invariance for any method that is going to be consistently successful in predicting supercell motion.

TABLE 2c. Same as Table 2a but for the 35 atypical supercell hodographs; see section 2a for definition of an atypical hodograph.

	ID	RB98	D98	DJ93	M76	C80
MAE (m s^{-1})	**3.6**	4.8	5.4	5.7	5.9	7.0
Student's *t*-test	—	−4.30	−3.86	−5.38	−5.31	−6.62
Best predicted (%)	—	31	31	17	17	11
Theta error (°)	14	23	23	20	20	28
Theta bias (°)	2	18	6	−17	−16	−23
SRH error (m^2 s^{-2})	34	46	48	63	62	88
SRH bias (m^2 s^{-2})	−10	15	−19	−61	−60	−86

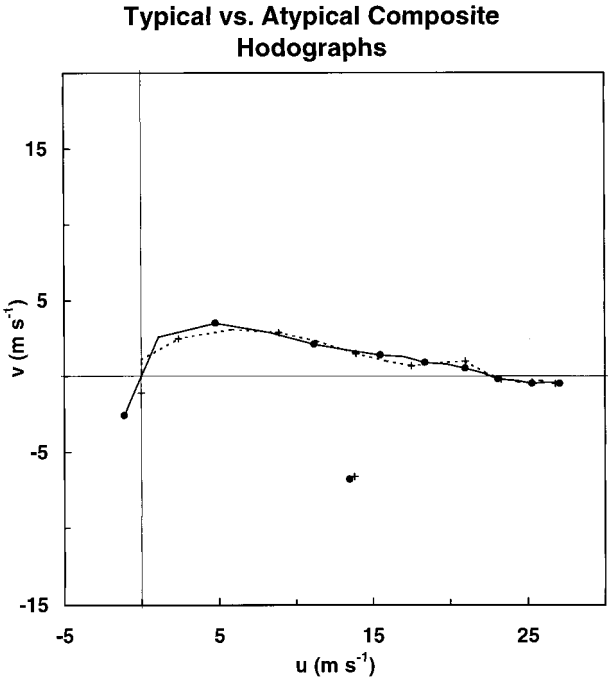

FIG. 5. Composite 0–8 km hodographs (m s^{-1}) for the 95 typical hodographs (solid line with solid circles at 1-km increments) and the 35 atypical hodographs (dashed line with plus signs at 1-km increments) discussed in the text. The composite storm motion for the typical composite hodograph is given by the solid circle, and the composite storm motion for the atypical composite hodograph is given by the plus sign.

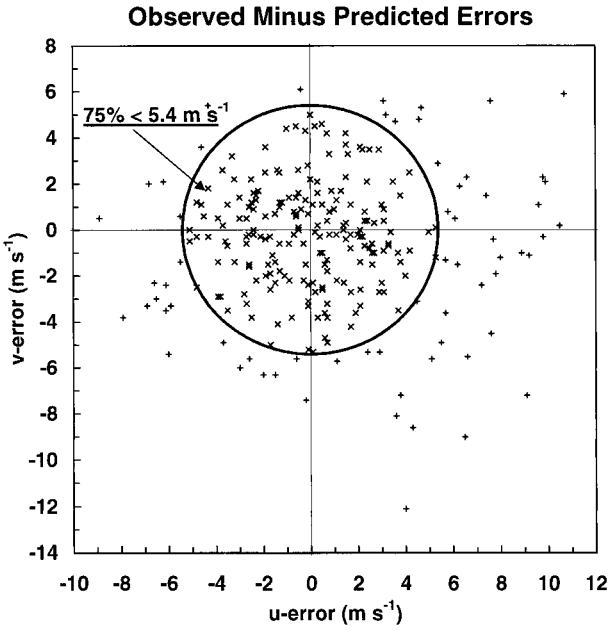

FIG. 6. Observed right-moving supercell motion minus the forecast motion by the ID method (m s^{-1}) for all 260 cases. Positive (negative) values indicate the supercell moved faster (slower) than what was predicted. Crosses (plus signs) indicate an error less than (greater than) 5.4 m s^{-1}.

The absolute errors in predicting supercell motion with the ID method (and other methods as well) were positively skewed (Fig. 4). [This did not affect the Student's *t*-test because the test statistic was made up of *differences* of the absolute errors (which can be approximated by a Gaussian distribution), and not the absolute errors themselves.] Most of this skewness was the result of those supercells whose motion was most poorly forecast, with the upper quartile of absolute errors covering a similar or greater range than the lowest 75% of the absolute errors. Moreover, many of these errors in the upper quartile (65%) had a tendency to occur as result of the supercell motion being underforecast by the ID method (Fig. 6)—defined here as positive errors in the x direction. However, there was no bias apparent in the absolute errors for the lowest 75% (these errors are contained in the circle in Fig. 6). Although the ID method offered significant improvement in predicting supercell motion when compared to other existing methods (Table 2, Fig. 4), there were times when it resulted in unacceptably large errors. These errors were not believed to be a systematic bias of the method, but rather were likely a result of factors not accounted for by the ID method. Understanding when the ID method might fail (discussed in section 3d below) is important to its correct application in these instances.

c. *Extending the ID method to left-moving supercells*

The ID method can also be applied to predicting the motion of left-moving supercells under the assumption that the propagation component is opposite to that for right-moving supercells [Eq. (2)]. This assumption is generally supported by both observational and modeling studies (Charba and Sasaki 1971; Klemp and Wilhelmson 1978; Weisman and Klemp 1986). Therefore, the same parameters were used in calculating the motion of left-moving supercells [Eq. (2)] as was done for the right-moving supercells [Eq. (1); see section 3a for the parameters].

The ID method was compared to the methods of RB98 and C80 for predicting the motion of left-moving supercells. Since the RB98 method is similar to the ID method, one can assume that left-moving supercells can be predicted by an offset to the left of the vertical wind shear vector they described. As discussed in section 1c, the C80 method can predict the motion of left-moving supercells given the proper orientation of the vertical wind shear; therefore, the effectiveness of that method was also evaluated. Upon comparison of the three methods, the ID method still produced the best overall results (Table 3), although the results were similar to those for the RB98 method. The ID method was statistically superior to the C80 method ($\alpha = 0.01$), but was not sta-

TABLE 3. Comparison statistics between the ID method and the other methods discussed in the text for the 30 left-moving supercell hodographs; otherwise the same as Table 2a.

	ID	RB98	C80
MAE (m s^{-1})	**3.5**	4.3	14.2
Student's *t*-test	—	−1.89	−11.04
Best predicted (%)	—	33	0
Theta error (°)	8	10	54
Theta bias (°)	1	−6	47
SRH error (m^2 s^{-2})	33	37	218
SRH bias (m^2 s^{-2})	−4	−15	218

tistically superior to that of RB98 at the $\alpha = 0.01$ significance level (it was significant at $\alpha = 0.05$). However, the ID method did result in the best prediction of the motion of the left-moving supercells 67% of the time when the two other methods were considered collectively (Table 3). All three methods produced reasonable predictions of the left-moving supercell motion given in Fig. 2e (i.e., errors <4 m s^{-1}).

d. Other factors influencing supercell motion—highly deviant storms

1) INTERNAL INFLUENCES: OUTFLOW–SHEAR INTERACTIONS

There are other factors that can influence supercell motion besides the two accounted for in the ID method. Another internal factor that may influence supercell motion results from the interaction of the thunderstorm outflow, or cold pool, with the low-level vertical wind shear—with the strength of the cold pool directly controlling the speed of propagation (e.g., the colder and deeper the cold pool, the faster its propagation speed relative to the surface wind). This has a tendency to produce an additional propagation component downshear of the convective updraft (Rotunno et al. 1988; Weisman 1993). A perusal of the meteorological literature as well as the hodographs obtained for this study suggests that HP supercells are more strongly influenced by this effect (as opposed to other types of supercells). Many times these storms are associated with—but independent of—bow echo configurations (Moller et al. 1990, 1994; Brooks and Doswell 1993; Conway et al. 1996; Klimowski et al. 1998). While not all HP storms are highly deviant in their motion, a substantial proportion of them do exhibit this tendency. This obviously complicates the problem of predicting supercell motion. Klemp (1987) suggests the effect of the cold pool may be ancillary compared to the advection and propagation effects discussed earlier; therefore, it may not always clearly manifest itself in the observed supercell motion.

In order to gain some understanding into the behavior of the deviant storms in the present study, an additional classification was made based on observations of hodographs and HP supercells in both the present study and the literature. As a result, hodographs in which observed supercell motion either deviated from the 0–6-km mean wind by more than 12.5 m s^{-1} or was greater than any of the winds on the 0–6-km hodograph were classified as highly deviant. It is noted that not all HP supercells deviated significantly from the mean wind; however, there was a tendency for this to occur. Nearly all of the DJ93 and journal hodographs put into this category were labeled by the original authors as HP or as being associated with a bow echo.

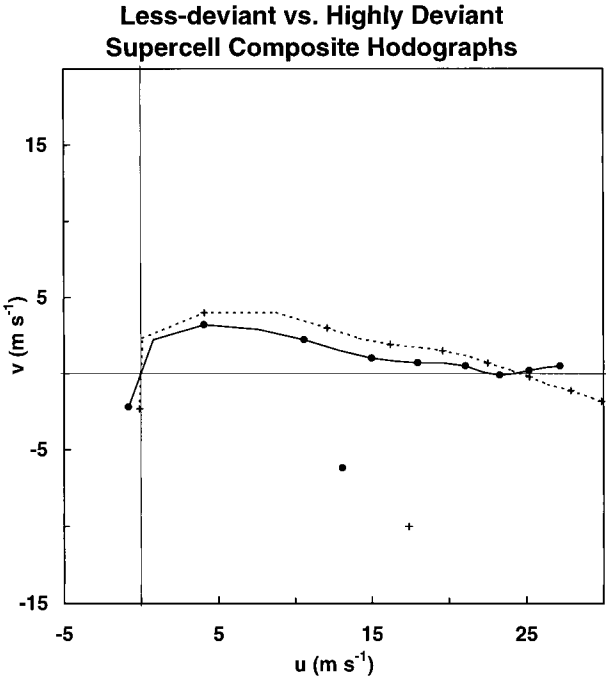

FIG. 7. Same as Fig. 5 except for the 225 less deviant right-moving supercell subset (solid line with solid circles) and the 35 highly deviant right-moving supercell subset (dashed line with plus signs) discussed in the text.

When applying the above criteria to the dataset of 260 right-moving supercells, 35 cases were selected. Of these, 31 (88%) were associated with the upper quartile of errors in predicting supercell motion by the ID method (outside of the circle in Fig. 6). The composite hodograph for these 35 highly deviant supercells, using the same procedure as was done in Fig. 5, is qualitatively similar to the 225 less deviant supercell composite (Fig. 7). However, the ID method forecast a motion within 1.3 m s^{-1} of the solid circle in Fig. 7 for both hodographs, which indicates a tendency for the highly deviant storms to move faster than predicted by the ID method. Moreover, the composite storm motion was 6 m s^{-1} greater for the highly deviant supercells when compared to the other 225 right-moving supercells; the direction of this deviation was opposite to the 0–3-km storm-relative inflow. The 0–6-km shear magnitude for the 35 (225) supercell composite hodograph was 30.6

m s^{-1} (27.7 m s^{-1}), and the 0–3-km SRH was 311 (195) m^2 s^{-2}. The fact that the SRH was much greater for the highly deviant supercells was related to both the faster storm motions and the slightly greater amount of shear. In addition, the composite storm motion of the 35 highly deviant supercells may be a reflection of a stronger mean wind, relative to that of the 225 supercell composite hodograph.

These results are generally consistent with Rasmussen and Straka's (1998) composite hodograph for HP supercells, although a direct comparison is not possible due to differences in case selection. First, both the direction and the magnitude of deviation of the composite storm motion for the 35 highly deviant supercells, relative to the storm motion of the 225 supercell composite, are similar to their findings for HP supercells. Examination of the individual highly deviant hodographs and motions in the present study indicated 22 (63%) of the supercells fit the highly deviant composite hodograph scenario, but the other 13 supercells displayed much more erratic movements relative to the composite. Second, the upper-level portion of the composite hodograph for the 35 highly deviant supercells (above 6 km) is characterized by veering winds—similar to Rasmussen and Straka's (1998) HP composite. This is opposed to backing winds in the 225 supercell composite, and both the LP and CL composites of Rasmussen and Straka (1998). Last, the upper-level storm-relative flow was slightly weaker for the 35 highly deviant storms when compared to the other 225 right-moving supercells. Despite these similarities, the composite hodographs in the present study exhibit substantially more low-level curvature—consistent with Brown (1993)—than those of Rasmussen and Straka (1998). Part of this may be due to differences either in the vertical resolution of the data or in the sampling of the supercell environments.

Although the upper-level storm-relative flow may help identify environments associated with highly deviant supercells, there still are situations when supercells will move in a highly deviant manner (such as in Fig. 7) that might be caused by other factors. For example, observations and modeling studies suggest supercell motion is dynamic rather than static. This generally manifests itself with a gradual increase in the storm motion with time. This evolution of the supercell motion may be due to (i) the storm gradually encountering a different environment (both shear and buoyancy), and (ii) an increase in the role of the storm outflow as the supercell matures, which may be related to the transition from the LP to the HP portion of the supercell spectrum. One problem with the present dataset is that storm motions were not calculated at the same point in the storm's life cycle for all supercells. Although in general the motions were obtained for the most intense phase, there may be cases when sampling occurred more toward the less outflow-dominated phase, while at other times sampling occurred after outflow had become a significant factor in modulating storm motion. It is apparent that one must be cognizant of the evolutionary stage of a given supercell and must anticipate possible changes in storm motion due to the factors just discussed—with an increased tendency for supercells to deviate in the direction opposite the low-level storm-relative inflow with time. The possibility of quantifying this deviation and determining when it is most likely is a subject of ongoing research.

2) External influences: atmospheric boundaries and orography

The ID method assumes supercell motion is largely governed by internal processes. However, external influences such as supercell interaction with fronts, drylines, outflow boundaries, orography, or other storms may contribute to the supercell motion, but these often are difficult to quantify a priori using just a hodograph.

Other studies have shown or implied the effect of atmospheric boundaries on supercell motion (Browning 1965; Weaver 1979; Weaver and Nelson 1982; Zehr and Purdom 1982; Markowski et al. 1998a). Using a numerical cloud model, Atkins and Weisman (1998) studied the interaction of simulated supercells with preexisting boundary layer convergence zones and found that the effect on storm motion was about 5 m s^{-1}. There are two likely processes that can occur as a supercell encounters a boundary. First, the vertical wind shear will be altered in the vicinity of a boundary relative to that at a location far removed from the boundary. Since supercell motion is in part dictated by the vertical wind shear, boundary-induced shear changes can explain some of the deviation of supercell motion upon interacting with a boundary. Second, convergence and buoyancy are usually enhanced near boundaries (e.g., Weaver 1979; Maddox et al. 1980), and as such, deep convective initiation is more likely. Therefore, given a small enough angle between the initial motion of a supercell and a boundary, the supercell may preferentially move along the boundary due to the development of new convective updrafts in this more favorable environment. Moreover, Weaver (1979) has shown that storms may propagate toward low-level convergence zones, resulting in little overall movement of the storm system. This may be especially important in environments characterized by large buoyancy and relatively weak shear.

One potential problem with quantifying the effects of atmospheric boundaries on predicting supercell motion is that soundings are not taken at a resolution that can represent the small-scale nature of the boundaries. Even higher-resolution WSR-88D and vertical wind profiler data may not always be sufficient to unravel the details of a the shear profile in the vicinity of a boundary, especially in the lowest 1–2 km. Furthermore, although the resolution of numerical weather prediction models

has increased to 20–30 km, difficulties in initialization will mean that at least the smaller-scale features are not well represented. Once again, it will be necessary for operational forecasters to be aware of atmospheric boundaries and how supercells may move upon interaction with such features.

Orography can also significantly influence supercell motion. The way in which this occurs may be difficult to assess, but experience with these types of situations may provide insight to the problem. For example, under certain situations enhanced convergence on either the windward or leeward side of an obstacle can favor convective development (Kuo and Orville 1973; Banta and Shaaf 1987; Hjelmfelt et al. 1994). This may lead to nearly stationary storms due to redevelopment or discrete propagation of new convection (e.g., Akaeda et al. 1995). Other examples of interactions between supercells and orography can be found in Bracken et al. (1998) and Keighton and Passetti (1998). It is interesting to note that in both of these cases, there was a period of consistent motion of the supercells, despite their proximity to elevated terrain. Examination of the vertical wind profiles of several ''orographically anchored'' supercell events suggests that they are favored when the vertical wind shear is marginally supportive of supercells (i.e., 0–6-km shear magnitude of 20–25 m s^{-1}).

4. Conclusions

The internal dynamics method was presented for predicting both right- and left-moving supercell motion. It is physically based, shear relative, Galilean invariant, and supported by numerous observational, modeling, and theoretical studies. The ID method was shown to be statistically superior to existing methods based on a 260 right-moving supercell dataset and a 30 left-moving supercell dataset. The MAE in predicting supercell motion was approximately 4 m s^{-1} for both datasets, with an improvement of 1 to 2 m s^{-1} over the other methods. When compared to methods that are not Galilean invariant, the ID method was especially useful in predicting supercell motion when the hodograph was *atypical*, that is, hodographs that displayed weak environmental winds or with vertical wind shear profiles not commonly observed. Other advantages of the ID method over most existing methods (except RB98) are that it always predicts off-hodograph motion for environments with unidirectional shear, and it is also capable of predicting stationary supercells, which has flash flood forecasting applications. Most importantly, the usefulness of the ID method depends on the existence of sufficient vertical wind shear for supercell processes to occur (refer back to Fig. 3a); it should not be applied in weak wind shear scenarios.

The following procedure can be used to predict supercell motion using the ID method and a hodograph:

- plot the 0–6 km non-pressure-weighted mean wind,
- draw the 0–0.5 to 5.5–6-km vertical wind shear vector,
- draw a line that both is orthogonal to the shear and passes through the mean wind,
- locate the right-moving supercell 7.5 m s^{-1} from the mean wind along the orthogonal line to the right of the vertical wind shear, and
- locate the left-moving supercell 7.5 m s^{-1} from the mean wind along the orthogonal line to the left of the vertical wind shear.

The key to easily applying this method is to view the hodograph from a vertical wind shear perspective as opposed to a mean wind perspective.

Based on these findings, we advocate predicting supercell motion using the ID method, at least as a starting point. This first estimate can then be modified given knowledge of what types of supercells are expected to develop, the depth of the troposphere, the location of atmospheric boundaries, and the effect that orography might have on evolving storms. Adjusting for the above factors is especially important since storm-relative flow concepts (e.g., SRH) require knowledge of supercell motion, and such information is important in distinguishing between the potential for tornadic versus nontornadic supercells.

Acknowledgments. The authors extend a special thanks to Jon Davies and Dr. Rodger Brown for providing their supercell datasets. The supercell data supplied by Gregory Gust, Ron Holmes, Vic Jensen, Robert Kleyla, George Phillips, Kim Runk, John Stoppkotte, Andrew Treloar, and Dr. John Monteverdi are also greatly appreciated. Discussions with Ms. Wendy Abshire and Drs. John Colquhoun, Art DeGaetano, Charles Doswell III, Erik Rasmussen, and Dan Wilks also significantly benefited the paper. The final manuscript was greatly improved by comments from Dr. John Weaver and two anonymous reviewers. Finally, the support provided by David Carpenter, the Meteorologist in Charge at the Rapid City National Weather Service Office, made this project possible.

APPENDIX

Supercell Occurrences from the Published Meteorological Literature

In order to produce a sufficiently large dataset of supercell cases, the published meteorological literature was searched for instances where supercells occurred within $\pm$ 3 h of sounding release time. In addition, either observed storm motions or figures that could be used to derive storm motions (e.g., radar images) were required. Hodographs were developed using the soundings reported in the literature, and for 13 cases, hodographs were digitized from figures contained in the literature. A total of 39 right-moving (Table A1) and 23 left-mov-

TABLE A1. Dates, soundings, and sources for the right-moving supercell occurrences gathered from the published meteorological literature. Where listed, figures from the references were used to develop the hodographs.

Date and sounding site/figure used	Supercell source
0000 UTC 25 May 1962, OKC	Newton and Fankhauser (1964)
1800 UTC 26 May 1963, TIK	Browning (1965)
0000 UTC 2 Jun 1965, OKC	Fankhauser (1971)
2300 UTC 25 Aug 1965, Fig. 6	Achtemeier (1969)
2300 UTC 26 Aug 1965, Fig. 6	Achtemeier (1969)
0000 UTC 17 Apr 1967, OKC	Colquhoun (1980)
0000 UTC 16 Jun 1970, DEN	Marwitz (1972)
1200 UTC 28 Aug 1973, ALB	Johns and Dorr (1996)
1200 UTC 25 May 1976, SEP	Moller et al. (1990)
0000 UTC 17 May 1978, SEP	Bluestein and Parks (1983)
0000 UTC 6 Jun 1979, Fig. 3c	Brown (1992)
0000 UTC 4 Jun 1980, LBF/OMA	Davies (1998)
1200 UTC 28 Feb 1987, JAN	Imy et al. (1992)
0000 UTC 5 May 1989, SEP	Moller et al. (1994)
0000 UTC 20 Jun 1990, TOP	Brooks and Doswell (1993)
1800 UTC 29 Nov 1991, UMN	Grant (1993)
2000 UTC 8 Mar 1992, OUN	Andra (1993)
0000 UTC 16 May 1992, OMA	Davies (1998)
0000 UTC 12 Jun 1992, MAF	Woodall (1993)
0000 UTC 28 Jun 1992, AMA	Davies (1998)
0000 UTC 5 Jul 1992, PAH	Glass and Truett (1993)
0000 UTC 5 Nov 1992, HAT	Vescio et al. (1993)
0000 UTC 31 Mar 1993, SIL	UCAR (1996)
0000 UTC 1 May 1993, DDC	Davies (1998)
0000 UTC 13 Jun 1993, LBF/OMA	Davies (1998)
2000 UTC 5 Mar 1994, NLC	Monteverdi and Johnson (1996)
0000 UTC 29 May 1994, SEP	UCAR (1996)
0000 UTC 30 May 1994, SEP	UCAR (1996)
0000 UTC 21 Jul 1994, OUN	UCAR (1996)
0000 UTC 17 Aug 1994, RAP	Bunkers (1996)
1200 UTC 17 Aug 1994, DDC	Conway et al. (1996)
0000 UTC 7 Sep 1994, GSO	Stuart (1997)
1200 UTC 18 Jan 1995, GGG	Calianese et al. (1996)
0500 UTC 6 Jul 1996, Fig. 4	Klimowski et al. (1998)
0000 UTC 15 May 1997, JAN	Cunningham and Wolf (1998)
0000 UTC 14 Aug 1997, DDC	Davies (1998)
0000 UTC 19 Aug 1997, AMA	Davies (1998)
0000 UTC 13 Sep 1997, DDC	Davies (1998)
1200 (0000) UTC 21(22) May 1998, LBF (OMA)	Davies (1998)

TABLE A2. Same as Table A1 but for the left-moving supercell occurrences.

Date and sounding site/figure used	Supercell source
0000 UTC 25 May 1962, OKC	Newton and Fankhauser (1964)
2000 UTC 3 Apr 1964, Fig. 12b	Charba and Sasaki (1971)
1800 (1900) UTC 22 Apr 1964, TIK	Hammond (1967)
1800 (0000) UTC 27 (28) May 1965, OKC	Harrold (1966)
0000 UTC 2 Jun 1965, OKC	Fankhauser (1971)
2300 UTC 25 Aug 1965, Fig. 6	Achtemeier (1969)
2300 UTC 26 Aug 1965, Fig. 6	Achtemeier (1969)
0000 UTC 17 Apr 1967, OKC	Haglund (1969)
2120 UTC 19 Apr 1972, Fig. 1	Brown et al. (1973)
1900 UTC 24 May 1973, Fig. 2	Lemon et al. (1978)
2000 UTC 30 May 1976, Fig. 1	Burgess (1981)
2310 UTC 19 Jul 1977, Fig. 2	Knupp and Cotton (1982)
2000 UTC 6 Jun 1979, Fig. 3c	Brown (1992)
1930 UTC 1 Aug 1981, Fig. 3	Kubesh et al. (1988)
0000 UTC 27 Apr 1984, OKC	Burgess and Curran (1985)
0000 UTC 28 Jun 1989, BIS	Brown and Meitín (1994)
2000 UTC 8 Mar 1992, SEP	UCAR (1996)
2000 UTC 8 Mar 1992, OUN	Andra (1993)
0000 UTC 26 May 1992, GGG/LCH	Nielsen-Gammon and Read (1995)
0000 UTC 11 Nov 1992, SEP	Kleyla (1993)
0000 UTC 7 May 1993, SEP	UCAR (1996)
0000 UTC 30 Jun 1994, LBF/TOP	Phillips (1994)
0000 UTC 7 Sep 1994, GSO	Stuart (1997)

ing (Table A2) supercell occurrences and motions were obtained.

REFERENCES

Achtemeier, G. L., 1969: Some observations of splitting thunderstorms over Iowa on August 25–26, 1965. Preprints, *Sixth Conf. on Severe Local Storms,* Chicago, IL, Amer. Meteor. Soc., 89–94.

Akaeda, K., J. Reisner, and D. Parsons, 1995: The role of mesoscale and topographically induced circulations in initiating a flash flood observed during the TAMEX project. *Mon. Wea. Rev.,* **123,** 1720–1739.

Andra, D. L., Jr., 1993: Observations of an anticyclonically rotating severe storm. Preprints, *17th Conf. on Severe Local Storms,* St. Louis, MO, Amer. Meteor. Soc., 186–190.

Atkins, N. T., and M. L. Weisman, 1998: The influence of pre-existing boundaries on supercell evolution. Preprints, *19th Conf. on Severe Local Storms,* Minneapolis, MN, Amer. Meteor. Soc., 334–337.

Banta, R. M., and C. B. Shaaf, 1987: Thunderstorm genesis zones in the Colorado Rocky Mountains as determined by traceback of geosynchronous satellite images. *Mon. Wea. Rev.,* **115,** 463–476.

Bluestein, H. B., and C. R. Parks, 1983: A synoptic and photographic climatology of low-precipitation severe thunderstorms in the southern plains. *Mon. Wea. Rev.,* **111,** 2034–2046.

——, and M. H. Jain, 1985: Formation of mesoscale lines of precipitation: Severe squall lines in Oklahoma during the spring. *J. Atmos. Sci.,* **42,** 1711–1732.

Bracken, W. E., L. F. Bosart, A. Seimon, K. D. Lapenta, J. S. Quinlan, and J. W. Cannon, 1998: Supercells and tornadogenesis over complex terrain: The Great Barrington (Massachusetts) Memorial Day (1995) tornado. Preprints, *19th Conf. on Severe Local Storms,* Minneapolis, MN, Amer. Meteor. Soc., 18–21.

Brooks, H. B., 1946: A summary of some radar thunderstorm observations. *Bull. Amer. Meteor. Soc.,* **27,** 557–563.

Brooks, H. E., and C. A. Doswell III, 1993: Extreme winds in high-precipitation supercells. Preprints, *17th Conf. on Severe Local Storms,* St. Louis, MO, Amer. Meteor. Soc., 173–177.

——, ——, and J. Cooper, 1994a: On the environments of tornadic and nontornadic mesocyclones. *Wea. Forecasting,* **9,** 606–618.

——, ——, and R. B. Wilhelmson, 1994b: The role of midtropospheric winds in the evolution and maintenance of low-level mesocyclones. *Mon. Wea. Rev.,* **122,** 126–136.

Brown, R. A., 1992: Initiation and evolution of updraft rotation within an incipient supercell thunderstorm. *J. Atmos. Sci.,* **49,** 1997–2014.

——, 1993: A compositing approach for preserving significant features in atmospheric profiles. *Mon. Wea. Rev.,* **121,** 874–880.

——, and R. J. Meitín, 1994: Evolution and morphology of two splitting thunderstorms with dominant left-moving members. *Mon. Wea. Rev.,* **122,** 2052–2067.

——, D. W. Burgess, and K. C. Crawford, 1973: Twin tornado cyclones within a severe thunderstorm: Single Doppler radar observations. *Weatherwise,* **26,** 63–71.

Browning, K. A., 1964: Airflow and precipitation trajectories within severe local storms which travel to the right of the winds. *J. Atmos. Sci.,* **21,** 634–639.

——, 1965: The evolution of tornadic storms. *J. Atmos. Sci.,* **22,** 664–668.

——, and R. J. Donaldson Jr., 1963: Airflow and structure of a tornadic storm. *J. Atmos. Sci.,* **20,** 533–545.

Bunkers, M. J., 1996: Examination of the preconvective environment associated with a severe nontornadic supercell: Variations in CAPE and SREH. Preprints, *18th Conf. on Severe Local Storms,* San Francisco, CA, Amer. Meteor. Soc., 703–707.

——, B. A. Klimowski, J. W. Zeitler, R. L. Thompson, and M. L. Weisman, 1998: Predicting supercell motion using hodograph techniques. Preprints, *19th Conf. on Severe Local Storms,* Minneapolis, MN, Amer. Meteor. Soc., 611–614.

Burgess, D. W., 1981: Evidence for anticyclonic rotation in left-moving thunderstorms. Preprints, *20th Conf. on Radar Meteorology,* Boston, MA, Amer. Meteor. Soc., 52–54.

——, and E. B. Curran, 1985: The relationship of storm type to environment in Oklahoma on 26 April 1984. Preprints, *14th Conf. on Severe Local Storms,* Indianapolis, IN, Amer. Meteor. Soc., 208–211.

——, and L. R. Lemon, 1991: Characteristics of mesocyclones detected during a NEXRAD test. Preprints, *25th Int. Conf. on Radar Meteorology,* Paris, France, Amer. Meteor. Soc., 39–42.

Byers, H. R., 1942: Nonfrontal thunderstorms. Miscellaneous Rep. 3, University of Chicago Press, 26 pp.

——, and R. R. Braham, 1949: *The Thunderstorm.* U.S. Government Printing Office, Washington, DC, 287 pp.

Calianese, E. J., Jr., A. R. Moller, and E. B. Curran, 1996: A WSR-88D analysis of a cool season, elevated high-precipitation supercell. Preprints, *18th Conf. on Severe Local Storms,* San Francisco, CA, Amer. Meteor. Soc., 96–100.

Charba, J., and Y. Sasaki, 1971: Structure and movement of the severe thunderstorms of 3 April 1964 as revealed from radar and surface mesonetwork data analysis. *J. Meteor. Soc. Japan,* **49,** 191–214.

Chisholm, A. J., and J. H. Renick, 1972: The kinematics of multicell and supercell Alberta hailstorms. Alberta Hail Studies, Research Council of Alberta Hail Studies Rep. 72-2, 53 pp. [Available from Alberta Research Council 4920-51 St., Red Deer, AB T4N 6K8, Canada.]

Colquhoun, J. R., 1980: A method of estimating the velocity of a severe thunderstorm using the vertical wind profile in the storm's environment. Preprints, *Eighth Conf. on Weather Forecasting and Analysis,* Denver, CO, Amer. Meteor. Soc., 316–323.

——, and D. J. Shepherd, 1989: An objective basis for forecasting tornado intensity. *Wea. Forecasting,* **4,** 35–50.

Conway, J. W., H. E. Brooks, and K. D. Hondl, 1996: The 17 August 1994 Lahoma, OK supercell: Issues of tornadogenesis and bow echo formation. Preprints, *18th Conf. on Severe Local Storms,* San Francisco, CA, Amer. Meteor. Soc., 52–56.

Cunningham, M., and P. Wolf, 1998: Supercell development over north-central Mississippi: Storm-scale changes to an unfavorable pre-storm environment. Preprints, *19th Conf. on Severe Local Storms,* Minneapolis, MN, Amer. Meteor. Soc., 328–331.

Darkow, G. L., 1969: An analysis of over sixty tornado proximity soundings. Preprints, *Sixth Conf. on Severe Local Storms,* Chicago, IL, Amer. Meteor. Soc., 218–221.

——, and D. W. McCann, 1977: Relative environmental winds for 121 tornado bearing storms. Preprints, *10th Conf. on Severe Local Storms,* Omaha, NE, Amer. Meteor. Soc., 413–417.

Davies, J. M., 1993: Small tornadic supercells in the central plains. Preprints, *17th Conf. on Severe Local Storms,* St. Louis, MO, Amer. Meteor. Soc., 305–309.

——, 1998: On supercell motion in weaker wind environments. Preprints, *19th Conf. on Severe Local Storms,* Minneapolis, MN, Amer. Meteor. Soc., 685–688.

——, and R. H. Johns, 1993: Some wind and instability parameters associated with strong and violent tornadoes. Part I: Wind shear and helicity. *The Tornado: Its Structure, Dynamics, Prediction, and Hazards, Geophys. Monogr.,* No. 79, Amer. Geophys. Union, 573–582.

Davies-Jones, R. P., 1984: Streamwise vorticity: The origin of updraft rotation in supercell storms. *J. Atmos. Sci.,* **41,** 2991–3006.

——, D. W. Burgess, and M. P. Foster, 1990: Test of helicity as a tornado forecast parameter. Preprints, *16th Conf. on Severe Local Storms,* Kananaskis Park, AB, Canada, Amer. Meteor. Soc., 588–592.

Dickins, J., 1994: South Australian supercells—A composite hodograph. Preprints, *Fourth Severe Thunderstorm Conf.,* Mt. Macedon, Victoria, Australia, Bureau of Meteorology, 1–9.

Droegemeier, K. K., S. M. Lazarus, and R. Davies-Jones, 1993: The

influence of helicity on numerically simulated convective storms. *Mon. Wea. Rev.*, **121,** 2005–2029.

Fankhauser, J. C., 1971: Thunderstorm–environment interactions determined from aircraft and radar observations. *Mon. Wea. Rev.*, **99,** 171–192.

——, and C. G. Mohr, 1977: Some correlations between various sounding parameters and hailstorm characteristics in northeast Colorado. Preprints, *10th Conf. on Severe Local Storms*, Omaha, NE, Amer. Meteor. Soc., 218–225.

Glass, F. H., and S. C. Truett, 1993: Observations of a splitting severe thunderstorm exhibiting both supercellular and multicellular traits. Preprints, *17th Conf. on Severe Local Storms*, St. Louis, MO, Amer. Meteor. Soc., 224–228.

Grant, B., 1993: Case study of the Nixa, Missouri tornado of 29 November, 1991. Preprints, *17th Conf. on Severe Local Storms*, St. Louis, MO, Amer. Meteor. Soc., 300–304.

Haglund, G. T., 1969: A study of a severe local storm of 16 April 1967. ESSA Tech. Memo. ERLTM-NSSL 44, 54 pp. [NTIS PB-184970.]

Hammond, G. R., 1967: Study of a left moving thunderstorm of 23 April 1964. ESSA Tech. Memo. IERTM-NSSL 31, 75 pp. [NTIS PB-174681.]

Harrold, T. W., 1966: A note on the development and movement of storms over Oklahoma on May 27, 1965. ESSA Tech. Memo. IERTM-NSSL 29, 51 pp. [NTIS AD-644899.]

Hjelmfelt, M. R., G. Kondrasuk, and D. Priegnitz, 1994: Effects of the Black Hills on mesoscale airflow and precipitation patterns. Preprints, *Sixth Conf. on Mesoscale Processes*, Portland, OR, Amer. Meteor. Soc., 566–569.

Imy, D. A., K. J. Pence, and C. A. Doswell III, 1992: On the need for volumetric radar data when issuing severe thunderstorm and tornado warnings. *Natl. Wea. Dig.*, **17,** 2–17.

Johns, R. H., 1984: A synoptic climatology of northwest-flow severe weather outbreaks. Part II: Meteorological parameters and synoptic patterns. *Mon. Wea. Rev.*, **112,** 449–464.

——, and R. A. Dorr Jr., 1996: Some meteorological aspects of strong and violent tornado episodes in New England and eastern New York. *Natl. Wea. Dig.*, **20,** 2–12.

——, J. M. Davies, and P. W. Leftwich, 1993: Some wind and instability parameters associated with strong and violent tornadoes. Part II: Variations in the combinations of wind and instability parameters. *The Tornado: Its Structure, Dynamics, Prediction, and Hazards, Geophys. Monogr.*, No. 79, Amer. Geophys. Union, 583–590.

Keighton, S., and V. Passetti, 1998: Anticipation and observation of a northern Arizona supercell over high terrain. Preprints, *16th Conf. on Weather Analysis and Forecasting*, Phoenix, AZ, Amer. Meteor. Soc., 124–126.

Kerr, B. W., and G. L. Darkow, 1996: Storm-relative winds and helicity in the tornadic thunderstorm environment. *Wea. Forecasting*, **11,** 489–505.

Klemp, J. B., 1987: Dynamics of tornadic thunderstorms. *Annu. Rev. Fluid Mech.*, **19,** 369–402.

——, and R. B. Wilhelmson, 1978: Simulations of right- and left-moving storms produced through storm splitting. *J. Atmos. Sci.*, **35,** 1097–1110.

Kleyla, R. P., 1993: A radar and synoptic scale analysis of a splitting thunderstorm over north-central Texas on November 10, 1992. Preprints, *17th Conf. on Severe Local Storms*, St. Louis, MO, Amer. Meteor. Soc., 211–214.

Klimowski, B. A., M. R. Hjelmfelt, M. J. Bunkers, D. Sedlacek, and L. R. Johnson, 1998: Hailstorm damage observed from the *GOES-8* satellite: The 5–6 July 1996 Butte–Meade storm. *Mon. Wea. Rev.*, **126,** 831–834.

Knupp, K. R., and W. R. Cotton, 1982: An intense, quasi-steady thunderstorm over mountainous terrain. Part II: Doppler radar observations of the storm morphological structure. *J. Atmos. Sci.*, **39,** 343–358.

Korotky, W. D., R. W. Przybylinski, and J. A. Hart, 1993: The Plainfield, Illinois, tornado of August 28, 1990: The evolution of synoptic and mesoscale environments. *The Tornado: Its Structure, Dynamics, Prediction, and Hazards, Geophys. Monogr.*, No. 79, Amer. Geophys. Union, 611–624.

Kubesh, R. J., D. J. Musil, R. D. Farley, and H. D. Orville, 1988: The 1 August 1981 CCOPE storm: Observations and modeling results. *J. Appl. Meteor.*, **27,** 216–243.

Kuo, J.-T., and H. D. Orville, 1973: A radar climatology of summertime convective clouds in the Black Hills. *J. Appl. Meteor.*, **12,** 359–368.

Lemon, L. R., D. W. Burgess, and R. A. Brown, 1978: Tornadic storm airflow and morphology derived from single-Doppler radar measurements. *Mon. Wea. Rev.*, **106,** 48–61.

Maddox, R. A., 1976: An evaluation of tornado proximity wind and stability data. *Mon. Wea. Rev.*, **104,** 133–142.

——, L. R. Hoxit, and C. F. Chappell, 1980: A study of tornadic thunderstorm interactions with thermal boundaries. *Mon. Wea. Rev.*, **108,** 322–336.

Markowski, P. M., E. N. Rasmussen, and J. M. Straka, 1998a: The occurrence of tornadoes in supercells interacting with boundaries during VORTEX-95. *Wea. Forecasting*, **13,** 852–859.

——, J. M. Straka, and E. N. Rasmussen, 1998b: The sensitivity of storm-relative helicity to small hodograph changes and resolution. Preprints, *19th Conf. on Severe Local Storms*, Minneapolis, MN, Amer. Meteor. Soc., 363–366.

Marwitz, J. D., 1972a: The structure and motion of severe hailstorms. Part I: Supercell storms. *J. Appl. Meteor.*, **11,** 166–179.

——, 1972b: The structure and motion of severe hailstorms. Part II: Multi-cell storms. *J. Appl. Meteor.*, **11,** 180–188.

——, 1972c: The structure and motion of severe hailstorms. Part III: Severely sheared storms. *J. Appl. Meteor.*, **11,** 189–201.

McCaul, E. W., Jr., 1991: Buoyancy and shear characteristics of hurricane–tornado environments. *Mon. Wea. Rev.*, **119,** 1954–1978.

——, and M. L. Weisman, 1996: Simulations of shallow supercell storms in landfalling hurricane environments. *Mon. Wea. Rev.*, **124,** 408–429.

Milton, J. S., and J. C. Arnold, 1990: *Introduction to Probability and Statistics: Principles and Applications for Engineering and the Computing Sciences.* McGraw-Hill, 700 pp.

Moller, A. R., C. A. Doswell III, and R. Przybylinski, 1990: High-precipitation supercells: A conceptual model and documentation. Preprints, *16th Conf. on Severe Local Storms*, Kananaskis Park, AB, Canada, Amer. Meteor. Soc., 52–57.

——, ——, M. P. Foster, and G. R. Woodall, 1994: The operational recognition of supercell thunderstorm environments and storm structures. *Wea. Forecasting*, **9,** 327–347.

Monteverdi, J. P., and S. Johnson, 1996: A supercell thunderstorm with hook echo in the San Joaquin Valley, California. *Wea. Forecasting*, **11,** 246–261.

Newton, C. W., and S. Katz, 1958: Movement of large convective rainstorms in relation to winds aloft. *Bull. Amer. Meteor. Soc.*, **39,** 129–136.

——, and J. C. Fankhauser, 1964: On the movements of convective storms, with emphasis on size discrimination in relation to water-budget requirements. *J. Appl. Meteor.*, **3,** 651–668.

Nielsen-Gammon, J. W., and W. L. Read, 1995: Detection and interpretation of left-moving severe thunderstorms using the WSR-88D: A case study. *Wea. Forecasting*, **10,** 127–140.

Phillips, G., 1994: Observation of a left-moving severe thunderstorm. NOAA/NWS CR WSR-88D Operational Note 94-06, 5 pp. [Available from NWS Central Region, 601 E. 12th St., Rm 1836, Kansas City, MO 64106-2897.]

Rasmussen, E. N., and D. O. Blanchard, 1998: A baseline climatology of sounding-derived supercell and tornado forecast parameters. *Wea. Forecasting*, **13,** 1148–1164.

——, and J. M. Straka, 1998: Variations in supercell morphology. Part I: Observations of the role of upper-level storm-relative flow. *Mon. Wea. Rev.*, **126,** 2406–2421.

Rotunno, R., and J. B. Klemp, 1982: The influence of the shear-induced pressure gradient on thunderstorm motion. *Mon. Wea. Rev.*, **110,** 136–151.

——, and ——, 1985: On the rotation and propagation of simulated supercell thunderstorms. *J. Atmos. Sci.,* **42,** 271–292.

——, ——, and M. L. Weisman, 1988: A theory for strong, long-lived squall lines. *J. Atmos. Sci.,* **45,** 463–485.

Stensrud, D. J., J. V. Cortinas Jr., and H. E. Brooks, 1997: Discriminating between tornadic and nontornadic thunderstorms using mesoscale model output. *Wea. Forecasting,* **12,** 613–632.

Stuart, N. A., 1997: The Wakefield, Virginia WSR-88D depiction of the 6 September 1994 split cell thunderstorm over southern Virginia. *Natl. Wea. Dig.,* **21,** 18–30.

Thompson, R. L., 1998: Eta model storm-relative winds associated with tornadic and nontornadic supercells. *Wea. Forecasting,* **13,** 125–137.

UCAR, 1996: *Anticipating Convective Storm Structure and Evolution*. University Corporation for Atmospheric Research, Cooperative Program for Operational Meteorology, Education, and Training (COMET), CD-ROM. [Available from COMET, P.O. Box 3000, Boulder, CO 80307-3000.]

Vescio, M. D., K. K. Keeter, G. Dial, P. Badget, and A. J. Riordan, 1993: A low-top weak-reflectivity severe weather episode along a thermal/moisture boundary in eastern North Carolina. Preprints, *17th Conf. on Severe Local Storms,* St. Louis, MO, Amer. Meteor. Soc., 628–632.

Weaver, J. F., 1979: Storm motion as related to boundary-layer convergence. *Mon. Wea. Rev.,* **107,** 612–619.

——, and S. P. Nelson, 1982: Multiscale aspects of thunderstorm gust fronts and their effects on subsequent thunderstorm development. *Mon. Wea. Rev.,* **110,** 707–718.

Weisman, M. L., 1993: The genesis of severe, long-lived bow echoes. *J. Atmos. Sci.,* **50,** 645–670.

——, and J. B. Klemp, 1982: The dependence of numerically simulated convective storms on vertical wind shear and buoyancy. *Mon. Wea. Rev.,* **110,** 504–520.

——, and ——, 1984: The structure and classification of numerically simulated convective storms in directionally varying wind shears. *Mon. Wea. Rev.,* **112,** 2479–2498.

——, and ——, 1986: Characteristics of isolated convective storms. *Mesoscale Meteorology and Forecasting,* P. S. Ray, Ed., Amer. Meteor. Soc., 331–358.

——, M. S. Gilmore, and L. J. Wicker, 1998: The impact of convective storms on their local environment: What is an appropriate ambient sounding? Preprints, *19th Conf. on Severe Local Storms,* Minneapolis, MN, Amer. Meteor. Soc., 238–241.

Wilks, D. S., 1995: *Statistical Methods in the Atmospheric Sciences.* Academic Press, 467 pp.

Woodall, G. R., 1993: The mesoscale environment of the 11 June 1992 severe storms in western Texas. *Natl. Wea. Dig.,* **18,** 22–31.

Zehr, R. M., and J. F. W. Purdom, 1982: Examples of a wide variety of thunderstorm propagation mechanisms. Preprints, *12th Conf. on Severe Local Storms,* San Antonio, TX, Amer. Meteor. Soc., 499–502.